JOURNAL OF MATERIALS SCIENCE 29 (1994) 2719–2724

Experimental determination of the stress-crack opening relation in fibre cementitious composites with a crack-tip singularity

V. C. LI, M. MAALEJ, T. HASHIDA
Advanced Civil Engineering Materials Research Laboratory, Department of Civil and Environmental Engineering, University of Michigan, Ann Arbor, MI 48109-2125, USA

in some of its fibre-reinforced composites, so that the crack-tip singular term cannot be neglected. In this regard, the J-based testing technique, originally proposed by Li *et al.* [5], is further developed in this paper in order to explicitly account for the crack-tip singularity while considering the bridging-process zone. The theoretical background behind the technique is briefly summarized in Section 2. The data-analysis procedure and experimental results for high-strength mortar reinforced with fibres are then reported.

2. A brief description of the J-based technique

This section provides the principle of the extended J-based technique. Li *et al.* [5] have proposed a novel J-based-fracture-testing technique to determine the tension–softening relationship used originally for characterizing concrete-fracture behaviour. This testing technique has the advantage of requiring only a simple stroke-controlled loading machine and it is relatively stable in comparison with direct uniaxial tensile tests. Since this proposal, the J-based technique has undergone extensive development. It has been applied by several researchers to a number of quasi-brittle materials (including concrete [6], fibre reinforced concrete [7–9] and rock [10–11]) in which the fracture process is primarily dominated by the formation of a fracture-process zone and in which the contribution of the crack-tip singularity to the total fracture energy is negligibly small.

A schematic of the stress distribution around the crack tip is presented in Fig. 1a for a material where the crack-tip singularity coexists with the fracture-process zone. The development of the fracture-process zone is characterized by a relationship between the stress, σ, and the crack-opening displacement, δ. This corresponds to the fictitious crack-process zone

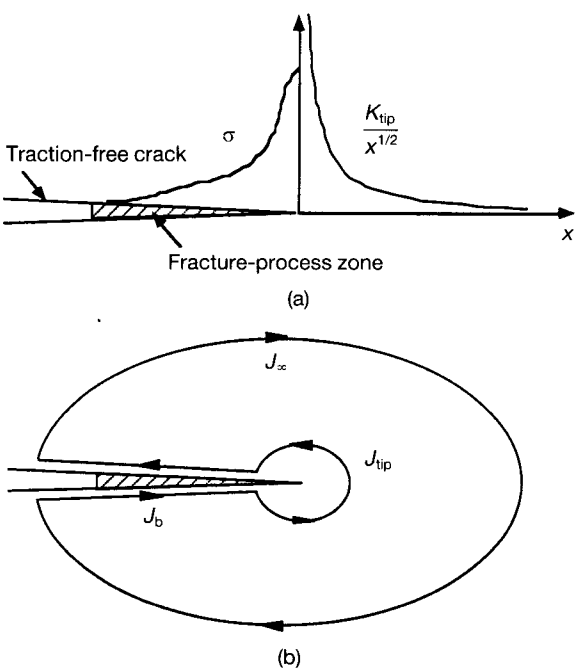

Figure 1 (a) A schematic plot of the stress distribution, and (b) the J-integral contour used for derivation of Equation 2.

of Hillerborg [4]. For the closed contour shown in Fig. 1b, the J-integral path-independent property [12] requires

$$J_\infty + J_b + J_{tip} = 0 \tag{1}$$

The J_∞-term represents the energy-release rate associated with far-field loading, and it contains information on the specimen geometry and applied load. J_{tip} is the crack-tip singularity term. Finally, J_b is the energy consumed by the development of the fracture-process zone. Applying the J-integral analysis to the terms J_{tip} and J_b for the material with the crack-tip singularity and fracture-process zone, Equation 1 can be expressed by

$$J_\infty = \int_0^{\delta_t} \sigma(\delta)\,d\delta + \frac{K_{tip}^2(1-\nu^2)}{E} \tag{2}$$

where δ_t is the crack-opening displacement measured at the original crack tip, K_{tip} is the crack-tip stress intensity factor, and E and ν are the composite's Young's modulus and Poisson's ratio, respectively. Differentiating Equation 2 with respect to δ_t, the stress, σ, may then be determined from

$$\sigma(\delta_t) = \frac{\partial}{\partial\delta_t}\left[J_\infty(\delta_t) - \frac{K_{tip}^2(1-\nu^2)}{E}\right] \tag{3}$$

When K_{tip} reaches the crack-tip toughness K_0, the fracture-process zone starts to grow according to the σ–δ relationship. Thus if J_∞ and K_0 can be determined, and δ_t can be obtained experimentally, then the σ–δ relationship can be derived from Equation 3. The J-integral value, J_∞, can be evaluated experimentally by conducting tests on a pair of specimens with differential notch lengths. Furthermore, the determination of the crack-tip toughness, K_0, can be obtained from the initial value of R-curves.

3. Experimental methods

The materials used in this study were high-strength mortar (HSM) and fibre-reinforced HSM. The dimensions and mechanical properties of the fibres used for reinforcement are given in Table I. The constituent materials of the matrix and their mix proportions are given in Table II. Type I Portland cement, silica sand (with a maximum grain size of 0.6 mm), silica fume and superplasticizer were used to form a HSM with a

TABLE I The dimensions and mechanical properties of fibres

Fibre	Fibre diameter (μm)	Fibre length (mm)	Elastic modulus (GPa)	Fibre strength (MPa)	Fibre density ($kg\,m^{-3}$)
Steel	150	6	200	2500	7800
Carbon	9.6	12.5	241	2800	2100

TABLE II Mortar mix proportions (by weight)

Cement	Sand	Silica fume	Superplasticizer	Water
1.00	0.75	0.10	0.02	0.27

water/cementitious ratio of 0.27. The compressive strength determined from three cylindrical specimens was 85.5 MPa. Carbon and steel fibres were used for reinforcing the matrix (with a fibre volume fraction of 1.5% for the carbon fibres, and 0.17% and 1.0% for the steel fibres).

The compact tension (CT) specimen illustrated in Fig. 2 was used to determine the σ–δ relationship of the materials by means of the J-based testing technique. An artificial notch with a root radius of 250 μm was introduced into each specimen. As a supplement to the J-based tests, uniaxial-tension tests were conducted on rectangular tensile specimens with a cross-section of 76 × 13 mm^2. The specimens were cast in Plexiglass moulds using a high-frequency vibration (150 Hz) in order to improve the packing of the material and to reduce air entrapment. After casting, they were allowed to harden at room temperature for one day prior to demoulding and then they were cured in water for four weeks before testing.

The fracture-toughness tests and uniaxial-tension tests were conducted in a hydraulic servo-controlled testing machine. The specimens were loaded to complete failure with a constant crosshead speed; the testing time was typically 10 min for all tests. The load, P, load-line displacement, δ_L, and crack-tip-opening displacement, δ_t, were monitored continuously. δ_L and δ_t were measured using linear-variable differential transducers (LVDTs). As is shown schematically in Fig. 2, a pair of LVDT holders were glued on the side surfaces of the specimen at the pre-notch tip. The relative displacement between the holders was measured on both specimen sides using LVDTs, and the two displacement values were averaged to determine δ_t. In some fracture-toughness tests, R-curve measurements were carried out using an unloading compliance method. Unloading and reloading cycles produced non-linear deformation, resulting in a significant hysteresis loop. Thus, a linearization procedure proposed in [13] was used to determine the specimen compliance. During the uniaxial tests, the relative displacement between two points along the loading axis was monitored to measure the elongation. The gauge length for the measurement was approximately 200 mm.

4. Results and discussion

In this section, the J-based technique briefly outlined above is applied to the experimental data for the HSM composites. In order to demonstrate the data-analysis procedure of the J-based technique, a set of experimental results for the carbon-fibre-reinforced HSM is presented first.

Fig. 3a shows average load versus load-line displacement curves for each crack length. Each curve represents an average of three repeated tests. Fig. 3b shows the relationship between the load-line displacement and the crack-tip-opening displacement (CTOD). The J-integral value is calculated from the set of P/B–δ_L curves (Fig. 3a) using the equation

$$J_\infty(\delta_L) = \frac{1}{(a_2 - a_1)} \int_0^{\delta_L} \left(\frac{P_1}{B} - \frac{P_2}{B} \right) d\delta_L \qquad (4)$$

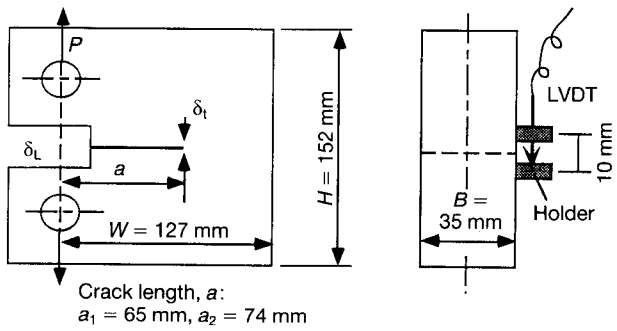

Figure 2 CT-specimen geometry and dimensions (LVDT, linear-variable differential transducer).

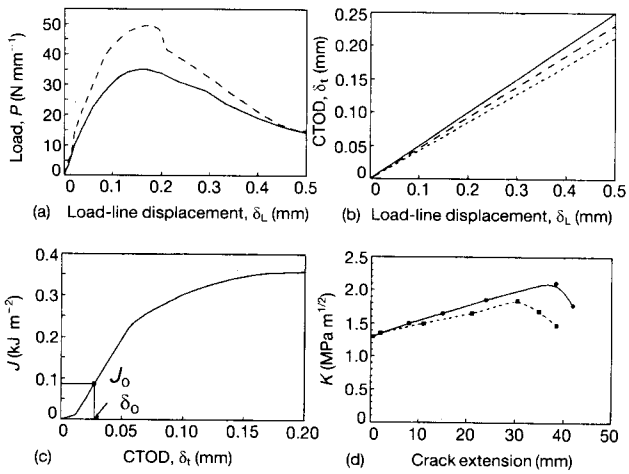

Figure 3 (a) Load versus displacement: (– – –) a_1 = 65 mm and (——) a_2 = 74 mm. (b) CTOD versus load-line displacement: (——) a_1 = 65 mm, (– – –) a_2 = 74 mm, and (— — —) the average of a_1 and a_2. (c) J-integral versus CTOD. (d) K-resistance curve: (——) a_1 = 65 mm and (– – –) a_2 = 74 mm. (All with 1.5% carbon-fibre HSM).

The result is plotted against the average CTOD in Fig. 3c. The total J-integral value is 0.36 kJ m^{-2}. The R-curve approach is used to determine the crack-tip toughness, K_0. An example of K-resistance curves is shown in Fig. 3d. The dimensionless specimen compliance and K formula for the CT specimen were taken from Newman's boundary collocation analysis [14] to construct the K-resistance curves. The initial value of the curve (1.33 MPa m$^{1/2}$) represents the critical stress intensity factor for advancing the crack against the modified matrix toughness, and thus it can be taken as the crack-tip toughness. Note that the decrease of the K-resistance curve at large crack extensions may be attributed to the crack propagation into the compression zone of the CT specimens. The J_0-value converted from the K_0-value using the equation $J_0 = K_0^2(1 - \nu^2)/E$ is indicated in the J versus δ_t plot in Fig. 3c. An experimental value of the effective Young's modulus, 20.5 GPa, was used in the calculation. It should be noted that the crack-tip toughness accounts for approximately one-quarter of the total toughness.

As in the original J-based technique [5], $J(\delta_t)$ is differentiated with respect to δ_t to obtain the bridging-stress–crack-opening-displacement curve, shown in

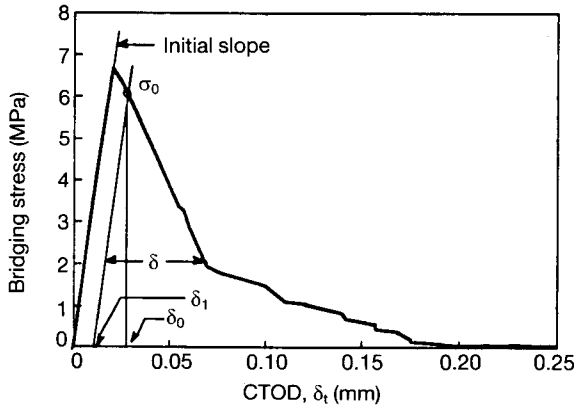

Figure 4 Bridging stress versus CTOD curve for 1.5% carbon-fibre HSM.

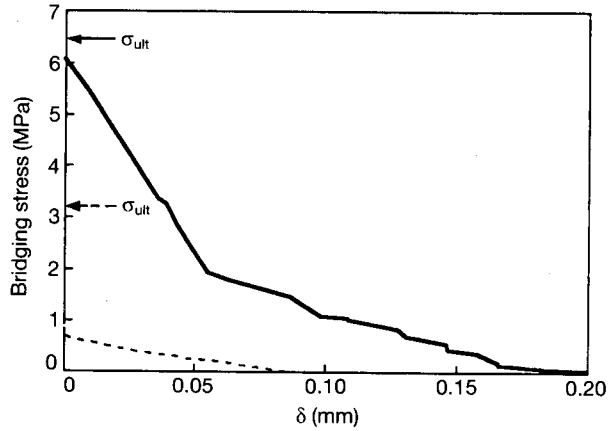

Figure 5 Deduced tension–softening curve for: (– – –) HSM, and (——) 1.5% carbon fibre HSM.

Fig. 4. The σ–δ_t curve initially rises to a peak, then it decreases with increasing δ_t. The rising portion of the curve is due to the presence of a strain between the LVDT holders. It can be interpreted as the sum of the elastic deformation and the distributed damage prior to localization of inelastic deformation onto the fracture-process zone, and therefore it should not be regarded as part of the bridging-stress–crack-opening-displacement relation [5]. In Fig. 3c, δ_0 represents the measured CTOD corresponding to the crack-tip toughness. This value defines a point (δ_0, σ_0) on the σ–δ_t curve (Fig. 4) through which a straight line parallel to the curve initial slope can be drawn. The portion of the σ–δ_t curve to the right of this line represents the true σ–δ curve. Numerically, the true σ–δ curve can be deduced from the σ–δ_t curve by applying the following correction to the crack opening,

$$\delta = \delta_t - \left[\delta_1 + \frac{\delta_0 - \delta_1}{\sigma_0}\sigma(\delta_t)\right] \quad (\text{for } \delta_t \geqslant \delta_0) \qquad (5)$$

where δ_1 is indicated in Fig. 4. Fig. 5 shows the corrected σ–δ curve, together with the result for the matrix alone, that is, for the HSM. The energy absorption of the carbon fibre in the post-peak region is higher than in the mortar. Microscopic observation of fracture surfaces showed that the fracture behaviour of the carbon fibre HSM is dominated by fibre rupture, and limited pull-out of the fibre was observed. Thus the higher bridging toughness of the carbon fibre HSM (with respect to HSM) may be attributed to this fibre pull-out. The experimental results regarding the J-based tests for all materials are summarized in Table III. In order to characterize the type of materials, the ratio of the crack-tip toughness to the total toughness, J_0/J_c, is indicated in Table III.

Using the stroke-control mode with the uniaxial-tensile test, no tension-softening behaviour was registered for the HSM and the carbon-fibre-HSM specimens. However, for each one of these materials, we expect the ultimate tensile strength to give an upper-bound value for the peak stress of the corresponding σ–δ curve. Fig. 5 shows that this is indeed the case. Moreover, evidence supporting the validity of the present J-based testing procedure can be observed in the steel-fibre–HSM composites where the post-peak behaviour is dominated by fibre pull-out.

A set of experimental results used in the computation of the σ–δ_t curve for the 0.17% steel-fibre–HSM composite is shown in Fig. 6. Uniaxial-tensile curves obtained for the steel-fibre–HSM composites, showed that the post-crack strength is lower than the ultimate strength. For composites where the ultimate strength is higher than the post-crack strength, there is the possibility of an underestimation of the post-peak composite strength, σ_{pc}. A theoretical model for the σ–δ relationship [15] based on the frictional fibre pull-out mechanism predicts that the post-peak composite strength is 0.66 MPa for the 0.17% steel-fibre–HSM and it is 3.89 MPa for the 1% steel-fibre–HSM (assuming an interfacial frictional bond strength of 10 MPa, and a snubbing coefficient of 0.8 [15]). The experimentally determined post-crack strength is close to the theoretical prediction. This may indicate that the observed post-crack strength

TABLE III A summary of the experimental results

Material	Fibre volume fraction (%)	Tensile strength[a] σ_{ult} (MPa)	Post-cracking strength[a] (MPa)	Effective Young's modulus (GPa)	Crack-tip toughness J_0 (kJ m^{-2})	Total toughness J_c (kJ m^{-2})	$\frac{J_0}{J_c}$
HSM	0	3.21	–	20.20	0.017	0.035	0.49
Carbon-fibre HSM	1.5	6.48	–	20.52	0.086	0.36	0.24
Steel-fibre HSM	0.17	3.43	0.82	19.70	0.019	0.47	0.04
Steel-fibre HSM	1	4.02	3.75	20.50	0.019	4.75	0.004

[a] Results of uniaxial-tension tests.

provides a good estimate of the true σ_{pc}-value. It should be particularly noted in Figs 7 and 8 that the deduced peak stress is close to the post-peak composite strength obtained from the uniaxial-tension tests. Moreover, it can be seen from the inset in Fig. 7 that, if the crack-tip toughness is neglected, the peak stress of the σ–δ curve deduced from the J-based method corresponding to the 0.17% steel-fibre HSM will be significantly overestimated. Table III indicates that, for this particular material, the ratio of the crack-tip toughness to the total toughness is about 4%.

It is therefore important to account for the crack-tip toughness in the determination of accurate σ–δ relationships in materials for which the ratio J_0/J_c is non-negligible. For the 1.0% steel-fibre-HSM composite where the crack-tip toughness is only 0.4% of the total toughness, the original J-based technique can provide a good estimate of the true σ–δ curve.

On the basis of the above observations, the experimental data of the bridging stress and the crack-tip toughness appear to be sufficient parameters for characterizing the fracture behaviour of fibre-reinforced HSM. Furthermore, the two characterizing parameters can be readily incorporated into numerical simulation codes, such as FEM (finite element method) and BEM (boundary element method), for analyses of fracture in fibre-reinforced high-strength concrete. Therefore, it is expected that the present J-based technique provides a basis for the fracture analysis of real structural components.

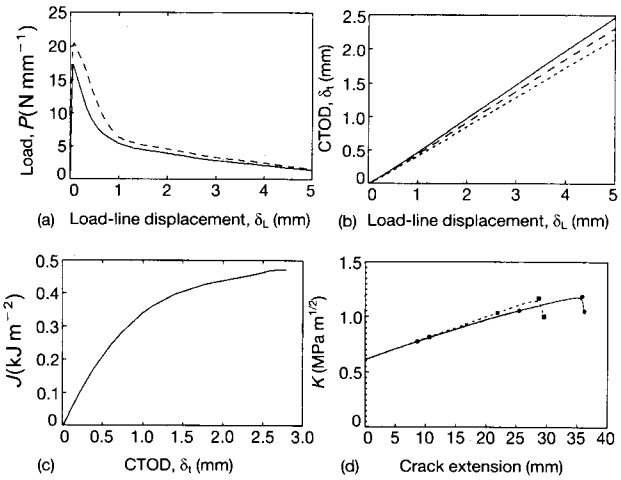

Figure 6 (a) Load versus displacement: (– – –) $a_1 = 65$ mm and (——) $a_2 = 74$ mm. (b) CTOD versus load-line displacement: (——) $a_1 = 65$ mm, (– – –) $a_2 = 74$ mm, and (— — —) the average of a_1 and a_2. (c) J-integral versus CTOD. (d) K-resistance curve: (——) $a_1 = 65$ mm and (– – –) $a_2 = 74$ mm. (All with 0.17% steel-fibre HSM).

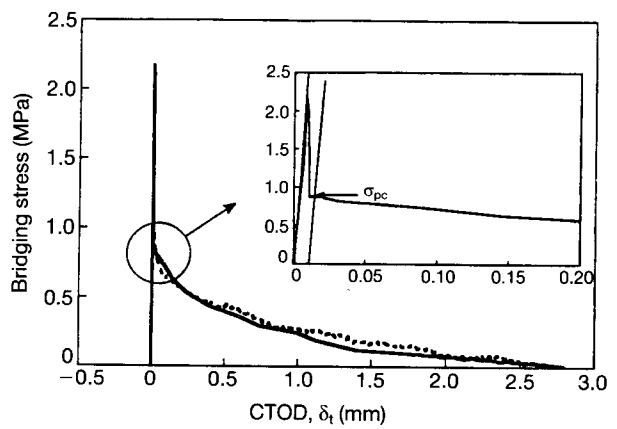

Figure 7 Bridging stress versus CTOD for a 0.17% steel-fibre HSM: (——) J-based result, and (···) uniaxial-tension result.

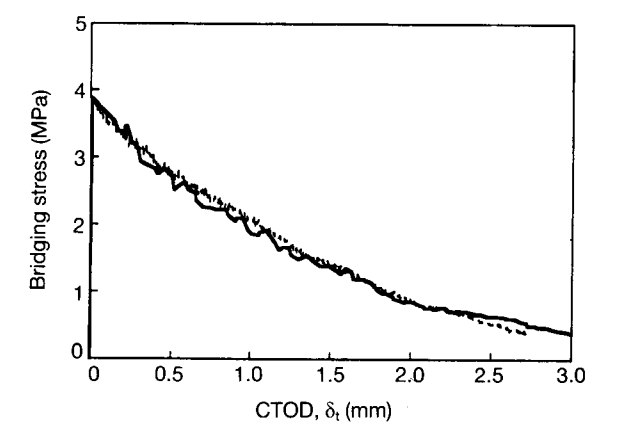

Figure 8 Bridging stress versus CTOD for a 1.0% steel-fibre HSM: (——) J-based result, and (···) uniaxial-tension result.

5. Conclusion

The J-based fracture-testing technique has been newly extended in order to cover HSM and its fibre-reinforced composites where the crack-tip toughness is comparable to the bridging toughness due to fracture-process-zone development. This method is even more essential for fibre-reinforced high-strength concrete where the crack-tip toughness can be considerably higher than in normal-strength concrete. On the basis of the J-integral analysis of the fracture-process zone with a crack-tip singularity, a testing procedure has been developed to determine the bridging-stress-crack-opening-displacement relation (σ–δ). This new technique has been applied to the experimental results of fracture tests conducted on HSMs reinforced with carbon and steel fibres. The σ–δ relationships deduced from the J-based technique have been compared with results of uniaxial-tensile tests and good agreements have been obtained, supporting the validity of the extended J-based fracture-testing method.

Acknowledgements

This research was supported by a research grant from the National Science Foundation (BCS 92 020 97) to the University of Michigan, Ann Arbor, USA.

References

1. S. P. SHAH, *Mater. Structures* **21** (1988) 145.
2. M. WECHARATANA and S. CHIMAMPHANT, in "Bonding in cementitious composites", Materials Research Society Symposium Volume, edited by S. Mindess and S. P. Shah (Materials Research Society, Pittsburgh, 1988) p. 114.
3. G. TOGNON and S. CANGIANO, in "Fracture toughness and fracture energy-test methods for concrete and rock", edited by H. Mihashi, H. Takahashi and H. Wittmann (Balkema, Rotterdam, 1989) p. 57.

4. A. HILLERBORG, in "Fracture mechanics of concrete", edited by F. H. Wittman (Elsevier, Amsterdam, 1983) p. 223.
5. V. C. LI, C. M. CHAN and C. K. Y. LEUNG, *Cement Concrete Res.* **17** (1987) 441.
6. S. TERAMURA, N. NOMURA, T. HASHIDA, H. TAKAHASHI and H. MIHASHI, in "Micromechanics of failure of quasi-brittle materials", edited by S. P. Shah, S. E. Swartz and M. L. Wang (Elsevier Applied Science, London, 1990) p. 463.
7. V. C. LI and R. WARD, in "Fracture toughness and fracture energy-test methods for concrete and rock", edited by H. Mihashi, H. Takahashi and H. Wittmann (Balkema, Rotterdam, 1989) p. 183.
8. C. K. Y. LEUNG and V. C. LI, *J. Mater. Sci.* **24** (1989) 854.
9. K. ROKUGO, M. IWASA, S. SEKO and W. KOYANAGI, in "Fracture of concrete and rock, recent developments", edited by S. P. Shah, S. E. Swartz and B. Barr (Elsevier, London, 1989) p. 513.
10. T. HASHIDA, in "Micromechanics of failure of quasi-brittle materials", edited by S. P. Shah, S. E. Swartz and M. L. Wang (Elsevier Applied Science, London, 1990) p. 233.
11. K. P. CHONG, V. C. LI and H. H. EINSTEIN, *Engng. Fract. Mech.* **34** (1989) 669.
12. J. R. RICE, *J. Appl. Mech.* **35** (1968) 379.
13. International Society for Rock Mechanics, *Int. J. Rock Mech. Min. Sci.* **25** (1988) 71.
14. J. C. NEWMAN, Jr. "Stress analysis of the compact specimen including the effects of pin loading", ASTM STP 560 (American Society for Testing and Materials, Philadelphia, 1974) p. 105.
15. V. C. LI, *J. Mater. Civil Engng* **4** (1992) 41.

Received 1 October 1992
and accepted 8 October 1993